LABORATORY INVESTIGATION

Adjuvant Thermal Accelerant Gel Use Increases Microwave Ablation Zone Temperature in Porcine Liver as Measured by MR Thermometry

Aaron W.P. Maxwell, MD, William K.C. Park, PhD, Grayson L. Baird, PhD, Edward G. Walsh, PhD, and Damian E. Dupuy, MD

ABSTRACT

Purpose: To determine the effects of a thermal accelerant gel on temperature parameters during microwave liver ablation.

Materials and Methods: Sixteen consecutive liver ablations were performed in 5 domestic swine under general anesthesia with (n = 8) and without (n = 8) administration of thermal accelerant gel. Ablation zone temperature was assessed by real-time MR thermometry, measured as maximum temperature (T_{max}) and the volume of tissue $\geq$ 60°C (V_{60}). Tissue heating rate, ablation zone shape, and thermal energy deposition using the temperature degree-minutes at 43°C (TDM43) index were also measured. Differences between groups were analyzed using generalized mixed modeling with significance set at $P = .05$.

Results: Mean peak ablation zone temperature was significantly greater with thermal accelerant use (mean T_{max}, thermal accelerant: 120.0°C, 95% confidence interval [CI] 113.0°C–126.9°C; mean T_{max}, control: 80.3°C, 95% CI 72.7°C–88.0°C; $P < .001$), and a significantly larger volume of liver tissue achieved or exceeded 60°C when thermal accelerant was administered (mean V_{60}, thermal accelerant: 22.2 cm^3; mean V_{60}, control: 15.9 cm^3; $P < .001$). Significantly greater thermal energy deposition was observed during ablations performed with accelerant (mean TDM43, thermal accelerant: 198.4 min, 95% CI 170.7–230.6 min; mean TDM43, control: 82.8 min, 95% CI 80.5–85.1 min; $P < .0001$). The rate of tissue heating was significantly greater with thermal accelerant use (thermal accelerant: 5.8 min ± 0.4; control: 10.0 min; $P < .001$), and accelerant gel ablations demonstrated a more spherical temperature distribution ($P = .002$).

Conclusions: Thermal accelerant use is associated with higher microwave ablation zone temperatures, greater thermal energy deposition, and faster and more spherical tissue heating compared with control ablations.

ABBREVIATIONS

CI = confidence interval, MW = microwave, T_{max} = maximum temperature, TDM43 = temperature degree-minutes at 43°C, V_{60} = volume of tissue $\geq$ 60°C

Image-guided thermal ablation is a potentially curative locoregional therapy for hepatic malignancies with treatment outcomes comparable to surgical resection for small lesions (1–3). For tumors > 3 cm in size, however, local tumor progression rates increase (4,5). Among patients who are not eligible for surgical resection, potential alternative therapeutic options include ablation combined with transarterial embolization (6,7), placement of multiple ablation antennae (8), or local administration of adjuvant agents.

Theoretical advantages of adjuvant agent use over other methods include the potential for targeted administration along irregular tumor margins or other sites deemed high risk for incomplete ablation, diminished procedural time, and lower cost. Hypertonic saline injection was the first such

From the The Warren Alpert Medical School of Brown University, 593 Eddy Street, Providence, RI 02903. Received September 30, 2019; final revision received December 23, 2019; accepted January 12, 2020. Address correspondence to A.W.P.M.; E-mail: aaron_maxwell@brown.edu; Twitter handle: @DoctorAWPM

W.C.K.P. is a cofounder and Chief Scientific Officer for Theromics, Inc (West Bridgewater, Massachusetts). D.E.D. is a cofounder and Chief Medical Officer of Theromics, Inc. None of the other authors have identified a conflict of interest.

From the SIR 2018 Annual Scientific Meeting.

J Vasc Interv Radiol 2020; ■:1–8

https://doi.org/10.1016/j.jvir.2020.01.010

EDITORS' RESEARCH HIGHLIGHTS

- This porcine study tested the effects of a thermal accelerant gel placed 1.5 cm away from a microwave antenna in the liver. The gel led to higher ablation-induced tissue temperatures, faster temperature increases, more spherical ablations, and larger volumes at cytotoxic temperatures ($\geq$ 60°C).
- All ablations were performed using an magnetic resonance-compatible generator and antenna at 100 W and a frequency of 2,450 MHz for 10 minutes.
- The feasibility study of 5 swine presents some limitations and opportunities: no gross or microscopic pathology was performed to certify the ablation shape and volume; the effect to surrounding organs was not evaluated. Indirect temperature measurements with magnetic resonance were performed without direct measurement. No data were provided on whether and where the gel used diffused in the liver. Finally, a nontumor model was used, limiting generalizability of the findings (though most ablation devices are tested in normal liver).

agent investigated, and its use has been shown to increase treatment effects following radiofrequency ablation owing to diminished impedance and higher ablation zone temperature (9). However, widespread adoption of this technique has been limited in part because of the risk of off-target ablation as well as unpredictable ablation zone size and geometry (10,11). To address these limitations, a viscous, protein-based adjuvant thermal accelerant gel has been developed for use during microwave (MW) ablation. The gel has previously been shown to significantly increase the ablation zone size in porcine liver, skeletal muscle, and lung (12,13). In vitro data from agarose phantoms suggest a temperature-based mechanism of action (14), though the effects of gel administration on temperature change in vivo have not been previously assessed.

Magnetic resonance (MR) thermometry is a noninvasive technique capable of measuring temperature in real time within a volume of interest with greater spatial resolution than conventional temperature measurement techniques, including thermocouple devices (15). Based on prior investigations, it is hypothesized that thermal accelerant gel administration would result in greater deposition of thermal energy within and surrounding the MW ablation antenna, resulting in higher ablation zone temperatures relative to ablations performed without the adjuvant agent. Accordingly, the purpose of the present investigation was to evaluate the in vivo effects of thermal accelerant gel on temperature change and distribution in porcine liver using real-time MR thermometry.

MATERIALS AND METHODS

Thermal Accelerant

The thermal accelerant gel is a proprietary formulation (Theromics, Inc, West Bridgewater, Massachusetts)

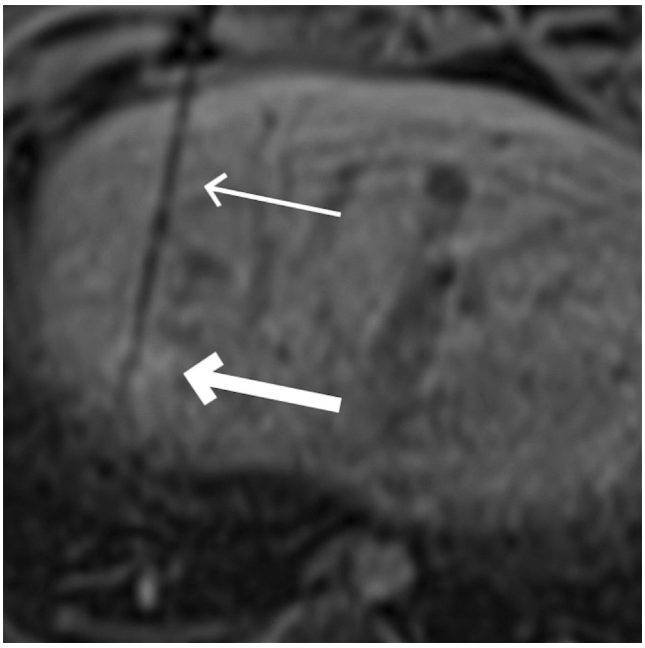

Figure 1. Axial T1-weighted volumetric interpolated breath-hold examination (VIBE) rapid scout image demonstrates a hyperintense thermal accelerant aliquot (thick arrow) following percutaneous injection into the right liver using a 5-F centesis catheter (thin arrow).

synthesized from fully biodegradable and biocompatible constituents. The gel has an aggregate viscosity of 3.48 kg/m/sec ± 0.08, a property that allows for targeted delivery without migration from the site of administration. Owing to its high protein and water content, the thermal accelerant is intrinsically visible on MR imaging without the use of intravenous contrast medium (Fig 1). The compound exists as a gel at both room and body temperature and can be directly delivered into or adjacent to the desired site of MW ablation using most commercially available needles and catheter devices.

MW Ablations

This study was performed between August 2017 and December 2017 following approval by the Institutional Animal Use and Care Committee. Five healthy castrated adult male *Sus scrofa domesticus* swine (median weight, 45 kg; range, 40–50 kg) were used. Swine were selected as the model organism owing to their high degree of anatomic and physiologic homology with humans. Before the ablation procedures, animals were housed in pairs within a dedicated animal research facility following 48 hours of acclimation. Nutrition was provided ad libitum until the midnight preceding the procedures, after which animals were to take nothing by mouth. All procedures were performed in a research facility with dedicated large animal procedural equipment.

General endotracheal anesthesia using 1%–4% inhaled isoflurane gas was administered by a doctor of veterinary medicine with 15 years of experience and additional qualifications in laboratory animal care. Continuous monitoring

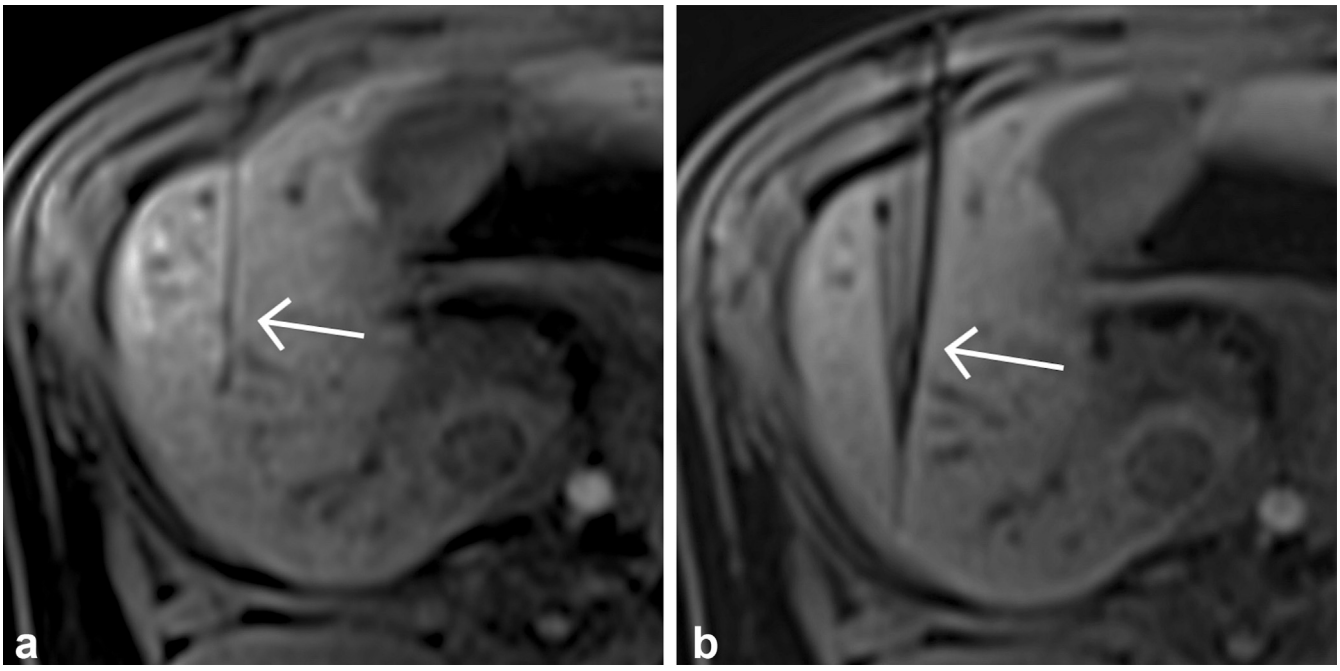

Figure 2. **(a)** Axial T1-weighted volumetric interpolated breath-hold examination rapid scout image demonstrates 5-F centesis catheter positioning before thermal accelerant injection into the right liver. **(b)** Following catheter removal, the MW ablation antenna is inserted near the deposited thermal accelerant aliquot, which is obscured by metallic susceptibility artifact.

including heart rate, pulse oximetry, and end-tidal capnography was employed for real-time assessment of animal well-being. Padded limb straps were used to safely secure animals in the supine position, and a warming blanket was placed for temperature regulation.

Sixteen MW liver ablations were successfully performed in 5 animals (8 ablations with thermal accelerant and 8 control ablations without thermal accelerant). Ablations were performed using MR imaging guidance on a 3.0T field strength Prisma scanner (Siemens Healthineers AG, Erlangen, Germany). Following induction of general anesthesia, a 4-channel flexible array receive coil was placed around the abdomen of the animal with an opening left for insertion of the ablation antenna and catheter for thermal accelerant delivery. Rapid gradient echo scout images were obtained before the procedure in each animal with vitamin E capsules affixed to the skin surface overlying the liver to act as fiducial markers. Once a safe percutaneous trajectory was identified, a small incision was made in the skin corresponding to the fiducial marker of interest.

For ablations performed using the thermal accelerant, a 15-cm 5-F centesis catheter (Cook Medical, Bloomington, Indiana) was advanced through the skin incision into the right hepatic lobe, which was chosen because of its larger size relative to other portions of the porcine liver. Ablation sites were chosen according to accessibility and remoteness from critical structures, such as the inferior vena cava and gallbladder. Following catheter placement, axial T1-weighted volumetric interpolated breath-hold examination (VIBE) rapid scout imaging was performed to confirm appropriate catheter positioning, followed by injection of 2 mL of thermal accelerant gel, a volume determined based on results of prior investigations (14). The catheter was then removed, and the MW antenna was advanced percutaneously into the liver with the feed point—located 1 cm proximal to the antenna tip—positioned within 1.5 cm of the thermal accelerant aliquot. This distance was chosen based on prior research demonstrating optimal performance of the accelerant gel when positioned at a distance from the MW energy feed point on the antenna (14). Before each ablation, a repeat rapid scout sequence was obtained to confirm appropriate antenna positioning (**Fig 2a, b**). Control ablations were performed similarly without injection of the accelerant gel.

All ablations were performed using an MR imaging–compatible generator and antennae (SurBlate; Vision Medical USA, Santa Clara, California) at a power of 100 W and a frequency of 2,450 MHz for a duration of 10 minutes. A maximum of 4 ablations were performed per animal by 1 of 2 authors (A.W.P.M., D.E.D., with 5 years and 25 years of experience in image-guided thermal ablation, respectively). The number of ablations per animal was chosen according to the volume of the right liver, and all ablations were performed a minimum of 5 cm apart to ensure no overlap between sequential treatments within the same animal. Immediately following the ablation procedures, the MW antenna was removed, and each animal was euthanized while under general anesthesia with a sodium pentobarbital solution (Fatal-Plus; Vortech Pharmaceutical Ltd, Dearborn, Michigan) administered intravenously by veterinary staff. All animals were monitored for complete cessation of

cardiopulmonary function following euthanasia before disposal.

MR Thermometry

Temperature mapping images were obtained during ablation procedures using a multiple gradient echo MR thermometry acquisition. The field of view was 243 × 300 mm with an acquisition matrix of 156 (phase) × 192 (read) and slice thickness of 5 mm (contiguous slices). Four echoes were acquired with echo times of 1.8 msec, 4.1 msec, 6.3 msec, and 8.6 msec. Repetition time was 40 msec with a flip angle of 15°. Fat suppression was employed along with respiratory gating. Temporal resolution was 1 minute. Before initiation of each ablation, a baseline dataset was obtained to serve as a reference for the subsequent generation of temperature change maps. On commencement of ablation, magnitude images and phase maps were obtained from 10 contiguous slices centered at the MW ablation antenna feed point with continuous acquisition throughout the ablation procedures. Given a total duration of 10 minutes per ablation, frequency changes resulting from B_0 field drift were negligible (16). Images were reconstructed using a least squares coil signal combination to provide both magnitude and phase images. Temperature change maps were then computed by fitting phase change against the baseline versus echo time on a pixel basis to obtain maps of frequency change, which were then scaled to temperature change using the factor of −0.01 ppm/°C (16–18). Temperature map production and subsequent analyses were performed using MATLAB (The MathWorks, Inc, Natick, Massachusetts).

Temperature Parameters

Ablation zone temperature was measured as the maximum absolute temperature achieved throughout the 10-minute treatment period at a location 1.5 cm from the MW antenna feed point (maximum temperature [T_{max}]). This distance was chosen to minimize uncertainty in temperature values owing to diminished T2* effects immediately adjacent to the antenna. Ablation zone temperature was also measured according to the volume of tissue within and surrounding the MW antenna that achieved or exceeded a predetermined temperature threshold of 60°C (volume of tissue ≥ 60°C [V_{60}]); this temperature was selected because it is a point of near-instantaneous and irreversible cytotoxicity (19). To calculate V_{60}, masks were generated on all slices corresponding to a minimum temperature of 60°C. The outer boundary was identified for each ablation, and slice volume was determined based on the number of pixels within the boundary multiplied by the size of the volume element. Total V_{60} was determined according to the sum of individual slice volumes, averaged by condition (thermal accelerant vs control). These temperature data were also used to calculate triaxial estimates (length × width × height) of the size of the cytotoxic core (> 60°C) within each ablation zone.

To determine the effects of accelerant gel administration on thermal energy disposition, the temperature degree-minutes at 43°C (TDM43) index was calculated from the time-temperature curves according to the formula:

$$TDM43 = \frac{\sum_{t=0}^{t=final}(T(t) - T_0)\Delta t}{43 - T_0}$$

where TDM43 is degree-minutes based on a 43°C reference, t is time, and T_0 is the starting temperature. This metric (20) provides a standardized interpretation of the temperature above a reference threshold and is used to compare temperature-based interventions in terms of the quantity of thermal energy deposition over time according to the equivalent number of minutes spent heating at 43°C, with longer duration corresponding to greater deposition.

Thermal Eccentricity

To determine the effect of thermal accelerant use on temperature distribution within the MW ablation zone, thermal eccentricity was measured. Given the baseline elliptical shape of ablation zones when thermal accelerant is not administered, the ellipse was chosen as the morphology after which the ablation zone was modeled. An elliptical fit was performed to image masks of pixels corresponding to peak temperatures ≥ 60°C surrounding the ablation antenna. Elliptical eccentricity values were then determined for each control and thermal accelerant ablation zone, with values ranging from 0 (perfect circle; less elongated) to 1 (straight line; more elongated). Routines for performing the elliptical fits were implemented according to the methods of Fitzgibbon and Pilu (21,22) using MATLAB scripts.

Statistical Analysis

A within-subjects, repeated measures block design was used where pigs served as their own controls. All modeling was accomplished using SAS 9.4 software (SAS Institute Inc., Cary, North Carolina) using the GLIMMIX procedure. Ablation zone temperature change was modeled by condition (thermal accelerant vs control) and time using a piecewise generalized linear mixed modeling with sandwich estimation where observations were nested within animals. Modeling of ablation volume and size, thermal energy deposition, rate of heating, TDM43, and eccentricity between conditions was accomplished also using generalized linear mixed modeling assuming lognormal and binomial distributions, respectively. Statistical significance was established at the .05 level, and all interval estimates were calculated for 95% confidence.

RESULTS

Average peak MW ablation zone temperature was significantly higher among ablations performed with the thermal accelerant gel (mean T_{max}, thermal accelerant: 120.0°C,

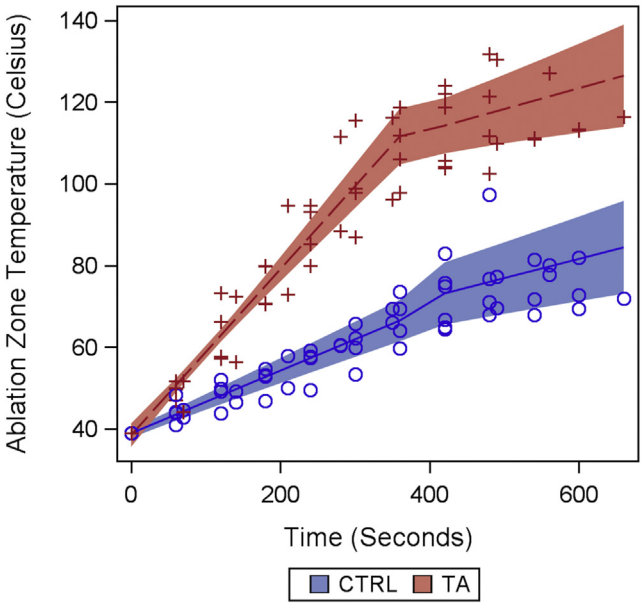

Figure 3. Thermal accelerant use during MW ablation in porcine liver was associated with a significantly greater mean ablation zone temperature (colored regions: 95% confidence bands). The rate of tissue heating was also higher with injection of the accelerant gel compared with control ablations, an effect greatest during the first 400 seconds of treatment. CTRL = control; TA = thermal accelerant.

95% confidence interval [CI] 113.0°C–126.9°C; mean T_{max}, control: 80.3°C, 95% CI 72.7°C–88.0°C; $P < .001$) (Fig 3). Throughout the treatment period, the rate of temperature change was significantly greater for ablations performed with the thermal accelerant gel compared with control ablations ($P < .0001$). As seen in Figure 3, this was most pronounced during the first 400 seconds of treatment, where temperature increase was more rapid for thermal accelerant ablations (slope = 0.20°C/s, 95% CI 0.18–0.23°C/s) than controls (slope = 0.07°C/s, 95% CI 0.06–0.09°C/s; $P < .0001$). After 400 seconds, temperature plateaued such that the average ablation zone temperature achieved using the accelerant gel was higher (T_{max}, thermal accelerant: 115.6°C, 95% CI 110.9°C–120.0°C) than controls (T_{max}, 74.5°C, 95% CI 72.5°C–76.4°C; $P < .0001$).

The administration of thermal accelerant gel resulted in a significantly greater quantity of thermal energy deposition as measured by TDM43 compared with control ablations (mean, thermal accelerant: 198.4 min, 95% CI 170.7–230.6 min; mean, control: 82.8 min, 95% CI 80.5–85.1 min; $P < .0001$). Similarly, the median volume of liver tissue that reached a cytotoxic temperature of ≥ 60°C (V_{60}) was significantly higher among thermal accelerant ablations (V_{60}, thermal accelerant: 22.2 cm^3, 95% CI 13.3–37.1 cm^3) than controls (median V_{60}, control: 15.9 cm^3, 95% CI 9.8–25.7 cm^3; $P < .0001$) (Fig 4).

There was a statistically significant increase in both width (mean, thermal accelerant: 46.2 mm, 95% CI 39.8–52.2 mm; mean, control: 38.7 mm, 95% CI 34.4–43.0 mm; $P = .03$) and height (mean, thermal accelerant: 35.8 mm, 95% CI 29.1–42.5 mm; mean, control: 28.7 mm, 95% CI 24.8–32.6 mm; $P = .03$) measurements within the ablation zone when thermal accelerant was administered relative to control ablations, defined according to a temperature threshold of ≥ 60°C. These increases resulted in a more spherical distribution of cytotoxic heating within the ablation zone, manifesting as significantly lower mean eccentricity values with accelerant gel use (mean, thermal accelerant: 0.66, 95% CI 0.62–0.72) compared with control ablations (mean, control: 0.79, 95% CI 0.73–0.84; $P = .002$) (Fig 5). There was no significant increase in long-axis ablation zone size between conditions (mean, thermal accelerant: 53.3 mm, 95% CI 42.7–63.9 mm; mean, control: 49.6 mm, 95% CI 42.8–56.5 mm; $P = .3$).

Ablations performed with accelerant gel were significantly faster than control ablations, achieving an equivalent magnitude of thermal energy deposition after a mean duration of 5.8 min ± 0.4 ($P < .001$) compared with control ablations. All planned ablations were completed, and there were no adverse events or premature animal deaths during the study period. Data are summarized in the Table.

DISCUSSION

When heat-based image-guided thermal ablation modalities such as MW ablation are employed with curative intent, the principal arbiter of oncologic effectiveness is temperature, with greater tissue heating beyond the cytotoxic threshold resulting in a larger volume of tumor necrosis (23). The mechanisms of tissue heating observed during MW ablation are complex and multiple, the result of interactions stemming from variations in MW energy transmission through different biologic tissues as well as the resultant phase transitions of water within and surrounding the ablation zone, including evaporation, diffusion, and condensation (24). The interplay of these variables with other external factors, such as heat sink effects (25), yields the final ablation zone volume, which in turn defines treatment margins and ultimately clinical outcomes (26,27).

The thermal accelerant gel evaluated in this investigation was designed to improve tissue heating during MW ablation primarily through a localized increase in dipole moment, an effect previously shown to significantly increase ablation zone volumes in porcine lung, kidney, liver, and skeletal muscle (12,13). The accelerant gel can be directly injected within or adjacent to an area of interest within soft tissue and has been previously demonstrated to increase both the rate and the magnitude of temperature change using an in vitro MW ablation phantom model (14). The in vivo effects of thermal accelerant administration on ablation zone temperature, however, have not previously been evaluated.

In the present investigation, the use of thermal accelerant gel percutaneously injected before MW liver

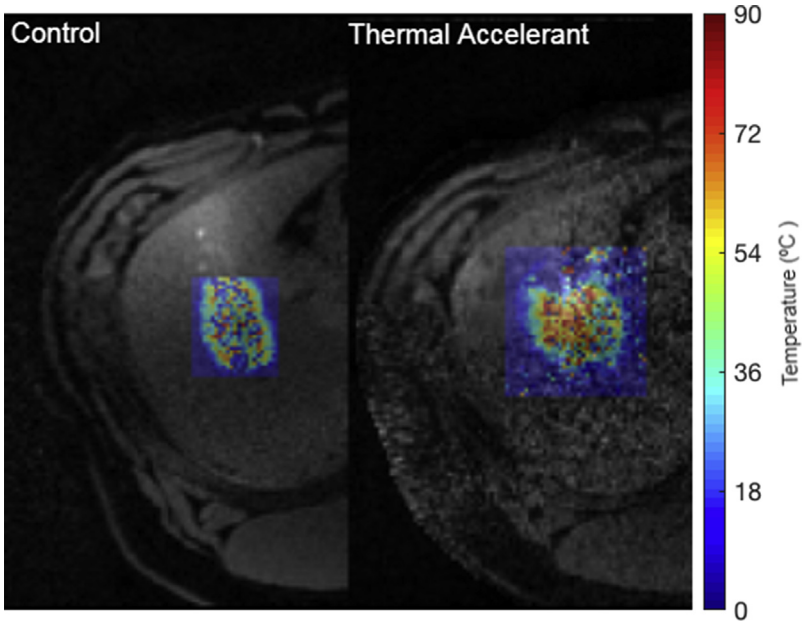

Figure 4. Representative T1-weighted axial MR image of the liver with colored temperature map overlay obtained during MW ablation. V_{60} was significantly greater when thermal accelerant gel was administered compared with control ablations.

ablation was found to significantly increase the average maximum temperature within the ablation zone by approximately 40°C, as measured by real-time MR thermometry. This increase in temperature corresponded to a greater than 2-fold increase in thermal energy deposition in the region surrounding the MW ablation antenna and an accompanying 38.4% increase in the volume of normal liver tissue that achieved or exceeded a cytotoxic temperature of 60°C. Together, these findings suggest that the ablation zone enlargement previously observed in several

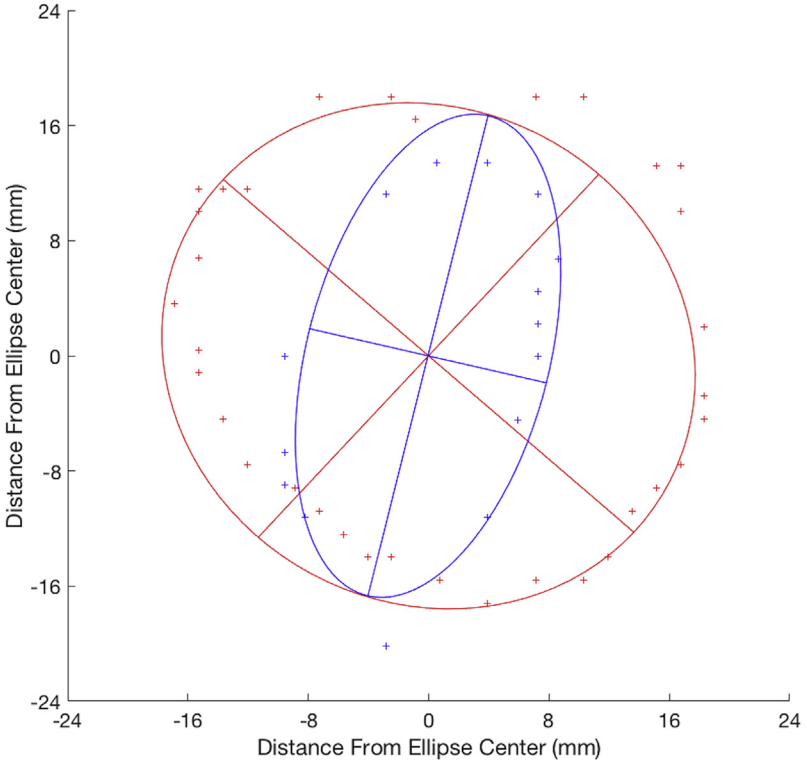

Figure 5. Thermal energy eccentricity of representative MW ablations performed without (blue) and with (red) thermal accelerant in the same animal. When the accelerant gel was administered, the volume of thermal energy within the ablation zone was significantly larger and more spherical in shape. Hash marks correspond to outer ablation zone boundaries, defined according to a temperature threshold of 60°C.

Table. Thermal Energy Parameters for MW Ablations Performed with and without Thermal Accelerant in Porcine Liver

	Thermal Accelerant	Control	*P*
T_{max}, °C	120.0 (113.0–126.9	80.3 (72.7–88.0)	< .001*
TDM43, min	198.4 (170.7–230.6)	82.8 (80.5–85.1)	< .0001*
V_{60}, cm^3	22.2 (13.3–37.1)	15.9 (9.8–25.7)	< .0001*
Width, 60°C, mm	46.2 (39.8–52.2)	38.7 (34.4–43.0)	.03*
Height, 60°C, mm	35.8 (29.1–42.5)	28.7 (24.8–32.6)	.03*
Length, 60°C, mm	53.3 (42.7–63.9)	49.6 (42.8–56.5)	.3
Eccentricity	0.66 (0.62–0.72)	0.79 (0.73–.84)	.002*

Note–Values presented as mean (95% confidence interval). MW = microwave; T_{max} = maximum temperature; TDM43 = temperature degree-minutes at 43°C; V_{60} = volume of tissue ≥ 60°C.
*Statistically significant ($P < .05$).

different organ systems (12,13) is primarily the result of increased temperature caused by thermal accelerant administration.

Higher average ablation zone temperature with accelerant gel use was also associated with faster tissue heating, with an approximately 42% reduction in time to achieve an average thermal energy deposition equivalent to that achieved without thermal accelerant gel injection. In clinical practice, this property may allow for shorter ablation treatments, which may result in an overall decrement in procedural duration. This may be particularly relevant when considering the placement of ≥ 1 additional ablation antennae for larger tumors or when combining percutaneous ablation with embolization-based procedures.

Temperature distribution within the ablation zone was also measured in this study. With thermal accelerant gel use, a more spherical distribution of cytotoxic heating was observed surrounding the MW antenna compared with the more elliptical shape of control ablations performed without accelerant gel. This finding may result from a decrease in reverse power along the shaft of the ablation antenna during treatment, itself reflecting enhanced MW energy absorption by the thermal accelerant gel leading to greater tissue heating further from the active feed point. This property has implications for focused ablation zone shaping with selective injection along the margins of irregular tumors or for targeting nearby satellite lesions that may fall outside the manufacturer specifications for ablation zone size using a single antenna. Evidence in favor of these potential applications includes the observed statistically significant increase in ablation zone width and height with thermal accelerant administration, itself reflecting the spatial relationship of MW antenna placement adjacent to—rather than within—the gel aliquot within the liver. Future studies evaluating different antenna-gel geometries are planned.

This study has several limitations. Because temperature was measured indirectly using MR thermometry techniques, the absolute magnitude of temperature change observed within the ablation zone may differ from what would be observed using direct methods of measurement. Similarly, as only liver ablations were performed, the effects of the thermal accelerant gel on temperature change in other organs remain unknown. The use of swine as a model organism may have impacted the observed results, and validation of these findings in tumor-bearing animals is necessary before translation into human clinical trials. Because samples for gross and microscopic pathologic evaluation were not obtained, the relationship between ablation zone temperature changes with and without the thermal accelerant and the extent of tissue necrosis remains unknown. Finally, though the obtained results suggest a thermal mechanism for the accelerant gel, additional factors not accounted for in this study, such as direct cytotoxicity, may also influence the observed increase in ablation zone size.

In conclusion, the use of an adjuvant thermal accelerant gel during MW ablation in porcine liver results in significant elevations in ablation zone temperature, thermal energy deposition, and both faster and more spherical tissue heating as measured by real-time MR thermometry.

REFERENCES

1. Forner A, Reig ME, de Lope CR, Bruix J. Current strategy for staging and treatment: the BCLC update and future prospects. Semin Liver Dis 2010; 30:61–74.
2. Peng ZW, Lin XJ, Zhang YJ, et al. Radiofrequency ablation versus hepatic resection for the treatment of hepatocellular carcinomas 2 cm or smaller: a retrospective comparative study. Radiology 2012; 262: 1022–1033.
3. Kang TW, Kim JM, Rhim H, et al. Small hepatocellular carcinoma: radiofrequency ablation versus nonanatomic resection—propensity score analyses of long-term outcomes. Radiology 2015; 275:908–919.
4. Shi J, Sun Q, Wang Y, et al. Comparison of microwave ablation and surgical resection for treatment of hepatocellular carcinomas conforming to Milan criteria. J Gastroenterol Hepatol 2014; 29: 1500–1507.
5. Urbonas T, Anderson EM, Gordon-Weeks AN, et al. Factors predicting ablation site recurrence following percutaneous microwave ablation of colorectal hepatic metastases. HPB 2019; 21:1175–1184.
6. Morimoto M, Numata K, Kondou M, Nozaki A, Morita S, Tanaka K. Midterm outcomes in patients with intermediate-sized hepatocellular carcinoma: a randomized controlled trial for determining the efficacy of radiofrequency ablation combined with transcatheter arterial chemoembolization. Cancer 2010; 116:5452–5460.
7. Peng ZW, Zhang YJ, Chen MS, et al. Radiofrequency ablation with or without transcatheter arterial chemoembolization in the treatment of hepatocellular carcinoma: a prospective randomized trial. J Clin Oncol 2013; 31:426–432.
8. Cazzato RL, De Marini P, Leclerc L, et al. Large nearly spherical ablation zones are achieved with simultaneous multi-antenna microwave ablation applied to treat liver tumours. Eur Radiol 2020; 30:971–975.
9. Lee JM, Han JK, Kim SH, et al. Comparison of wet radiofrequency ablation with dry radiofrequency ablation and radiofrequency ablation using hypertonic saline preinjection: ex vivo bovine liver. Korean J Radiol 2004; 5:258–265.
10. Schmidt D, Trubenbach J, Brieger J, et al. Automated saline-enhanced radiofrequency thermal ablation: initial results in ex vivo bovine livers. AJR Am J Roentgenol 2003; 180:163–165.
11. Lee JM, Kim YK, Lee YH, Kim SW, Li CA, Kim CS. Percutaneous radiofrequency thermal ablation with hypertonic saline injection: in vivo study in a rabbit liver model. Korean J Radiol 2003; 4:27–34.
12. Maxwell AWP, Park WKC, Baird GL, Martin DW, Lombardo KA, Dupuy DE. Effects of a thermal accelerant gel on microwave ablation zone volumes in lung: a porcine study. Radiology 2019; 291:504–510.

13. Park WKC, Maxwell AWP, Frank VE, et al. The in vivo performance of a novel thermal accelerant agent used for augmentation of microwave energy delivery within biologic tissues during image-guided thermal ablation: a porcine study. Int J Hyperthermia 2018; 34:11–18.
14. Park WK, Maxwell AW, Frank VE, et al. Evaluation of a novel thermal accelerant for augmentation of microwave energy during image-guided tumor ablation. Theranostics 2017; 7:1026–1035.
15. Winter L, Oberacker E, Paul K, et al. Magnetic resonance thermometry: methodology, pitfalls and practical solutions. Int J Hyperthermia 2016; 32: 63–75.
16. Bertsch F, Mattner J, Stehling MK, et al. Non-invasive temperature mapping using MRI: comparison of two methods based on chemical shift and T1-relaxation. Magn Reson Imaging 1998; 16:393–404.
17. Ishihara Y, Calderon A, Watanabe H, et al. A precise and fast temperature mapping using water proton chemical shift. Magn Reson Med 1995; 34: 814–823.
18. Hindman JC. Proton resonance shift of water in the gas and liquid states. J Chem Phys 1966; 44:4582–4592.
19. Chu KF, Dupuy DE. Thermal ablation of tumours: biological mechanisms and advances in therapy. Nat Rev Cancer 2014; 14:199–208.
20. Sapareto SA, Dewey WC. Thermal dose determination in cancer therapy. Int J Radiat Oncol Biol Phys 1984; 10:787–800.
21. Fitzgibbon AW, Fisher RB. A buyer's guide to conic fitting. *Proceedings of the 6th British Conference on Machine Vision (Vol 2)*. Birmingham, United Kingdom. Guildford, UK: BMVA Press; 1995. p. 513–522.
22. Pilu M, Fitzgibbon AW, Fisher RB. Ellipse-specific direct least-square fitting. *Proceedings of 3rd IEEE International Conference on Image Processing (Vol III)*. New York, NY: The Institute of Electrical and Electronics Engineering, Inc; 1996.
23. Simon CJ, Dupuy DE, Mayo-Smith WW. Microwave ablation: principles and applications. Radiographics 2005; 25(Suppl 1):S69–S83.
24. Yang D, Converse MC, Mahvi DM, Webster JG. Measurement and analysis of tissue temperature during microwave liver ablation. IEEE Trans Biomed Eng 2007; 54:150–155.
25. Yu NC, Raman SS, Kim YJ, Lassman C, Chang X, Lu DS. Microwave liver ablation: influence of hepatic vein size on heat-sink effect in a porcine model. J Vasc Interv Radiol 2008; 19:1087–1092.
26. Shady W, Petre EN, Do KG, et al. Percutaneous microwave versus radiofrequency ablation of colorectal liver metastases: ablation with clear margins (A0) provides the best local tumor control. J Vasc Interv Radiol 2018; 29:268–275.e1.
27. Shady W, Petre EN, Gonen M, et al. Percutaneous radiofrequency ablation of colorectal cancer liver metastases: factors affecting outcomes—a 10-year experience at a single center. Radiology 2016; 278:601–611.